Supplementary Information

N, O co-doped Fe-N_X catalysts with efficient bifunctional properties for Zinc-air battery applications

Chengxiao Xu,[a] Daming Li,[a] Shuaiquan Zhao,[a] Yuchen Zhang,[a] Yuzheng Li,[a] Jinjie Zhang, [a] Bo Liu,[a] Peipei Huo,*[a]

[a] School of Physics and Optoelectronic Engineering, Shandong University of Technology, Xincun West Road 266, Zibo 255000, China;

* Corresponding authors. *E-mail* addresses: peipeihuo@sdut.edu.cn (P. Huo).

1.Experimental section

1.1 Materials

2-Methylimidazole, having a purity of 98%, was purchased from Shanghai Aladdin Biochemical Technology Co., Ltd, Zinc acetate, with a purity of 99.9%, was obtained from Shanghai Aladdin Biochemical Technology Co., Ltd., KOH (AR) was sourced from Sinopharm Chemical Reagent Co., Ltd., located in Shanghai, China, 2-Methylimidazole (98%) were obtained from Shanghai Aladdin Biochemical Technology Co. Ltd. (Shanghai, China), , Ltd (Shanghai, China), PT20 were obtained from Suzhou Sinero Technology Co. Ltd (Suzhou, China), RuO_2 was purchased from Suzhou Sinero Technology Co., Ltd, Iron citrate (AR) was obtained from Shanghai Macklin Biochemical Technology Co., Ltd, Zinc oxide, with a purity of 99.8%, was sourced from Shanghai Aladdin Biochemical Technology Co., Ltd, Polyacrylonitrile and N, N-Dimethylformamide (DMF), with a purity of 99.5%, were purchased from Shanghai Aladdin Biochemical Technology Co., Ltd, HCl (AR) was sourced from Sinopharm Chemical Reagent Co., Ltd.

1.2 Characterization and measurements

The materials were characterized using various techniques. SEM images were captured using an FEI Quanta 250 instrument, while TEM images were obtained from an FEI Talos F200X. XRD patterns were recorded on a Rigaku SmartLab SE system, with scanning angles ranging from 5° to 90°. The surface elemental composition was analyzed by XPS on a Thermo Scientific K-Alpha spectrometer. Raman spectroscopy measurements were performed using a WJGS-034 HR Evolution Horiba instrument. Additionally, nitrogen adsorption and desorption isotherms were evaluated using a Quantachrome Autosorb IQ3 physical adsorption analyzer, with a desorption temperature of 300°C.

1.3 Electrochemical measurements

Electrochemical evaluations were conducted on a CHI 760E workstation using a three-electrode setup. Disperse 4 mg of catalyst into 0.99 mL of anhydrous ethanol, and concurrently introduce 10 μL of Nafion solution. Subject this mixture to ultrasonication for a duration of 30 minutes to procure a homogeneous catalyst ink. A 10-microliter aliquot of the ink was evenly deposited onto a 5 mm glassy carbon electrode. Ensure that the loading on the rotating disk electrode is 0.2 mg/cm^2.The auxiliary electrode was a graphite rod, and the reference electrode was an Ag/AgCl electrode immersed in saturated KCl solution. Linear sweep voltammetry (LSV) was performed at a scan rate of 10 millivolts per second in a 0.1M KOH solution saturated with N_2 and O_2. The Tafel slope was determined using the equation $\eta = b\log(j) + a$. A current-time (i-t) test was conducted at 0.6V for 40,000 seconds, with a rotation speed of 1,600 RPM. Cyclic voltammetry (CV) measurements were taken in 0.1M KOH solutions saturated with either N_2 or O_2. The ORR polarization curve was obtained by subtracting the background current from the O2-saturated current.

To assemble the zinc-air battery (ZAB), the catalyst ink was prepared by dispersing 1 mg of FeN_X@N,O-CNF-act or Pt/C+RuO_2 in 1 mL ethanol and 10 uL of Nafion, followed by ultrasonic treatment for less than 30 minutes. Then, all of the ink were coated onto a carbon cloth to achieve a catalyst loading of 1 milligram per square centimeter, serving as the cathode. The anode was a polished

zinc surface, and the electrolyte was a mixture of 6 M KOH and 0.2 M $Zn(AC)_2$. The assembled ZAB was stabilized for 2 h at room temperature before testing.

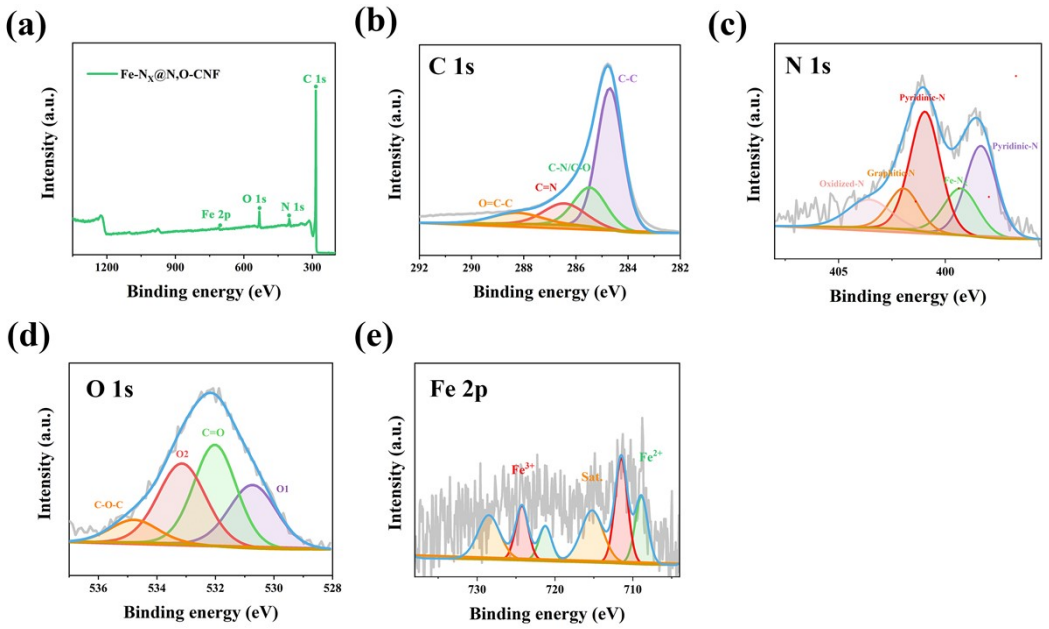

Fig. S1 XPS spectra (a) survey (b-d) C 1s, N 1s, O 1s and Fe 2p of Fe-N$_X$@N,O-CNF.

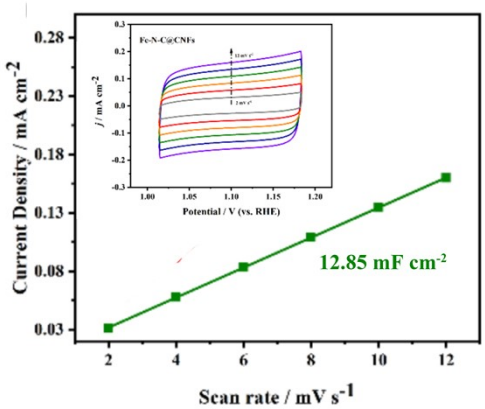

Fig. S2 C_{dl} and non-faradic current density at different scan rates of Fe-N$_X$@N,O-CNF.

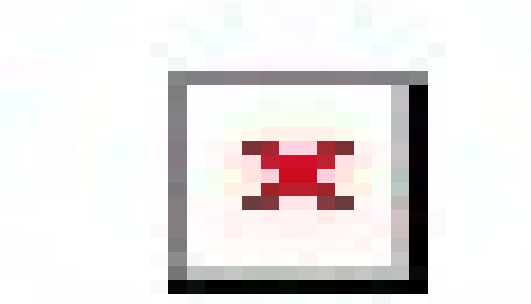

Fig. S3 LSV curves collected at different rotation speeds and corresponding K-L plots of Fe-N$_X$@N,O-CNF.

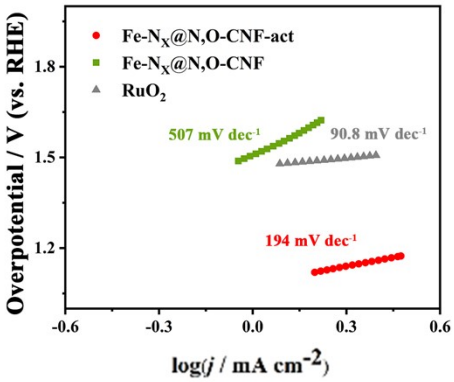

Fig. S4 Tafel slope plot.

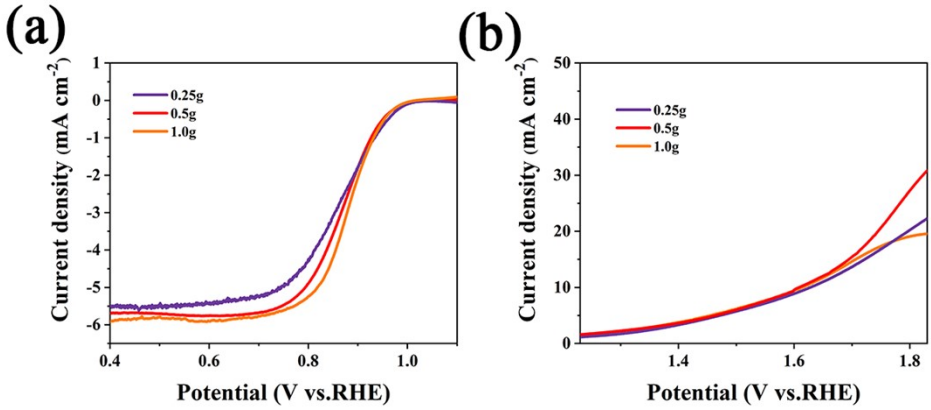

Fig. S5 (a) ORR and (b) OER polarization curves of 0.25-Fe-N$_X$@N,O-CNF-act, 0.5-Fe-N$_X$@N,O-CNF-act and 1.0-Fe-N$_X$@N,O-CNF-act.

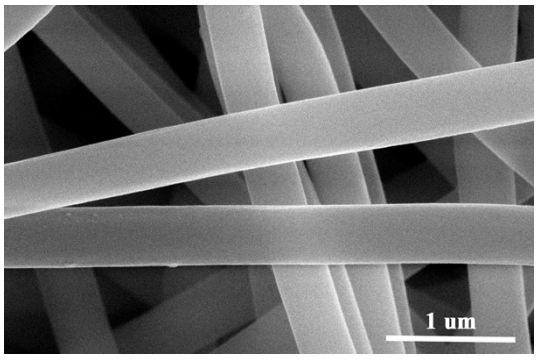

Fig. S6 SEM image of CNF.

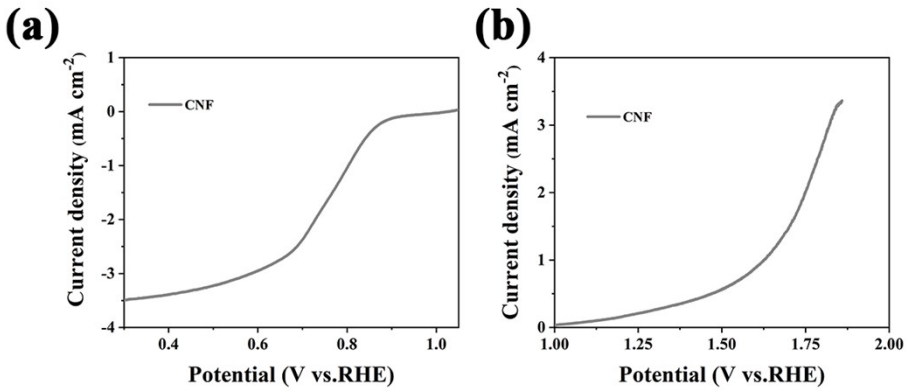

Fig. S7 LSV curves of (a) ORR and (b) OER for CNF.

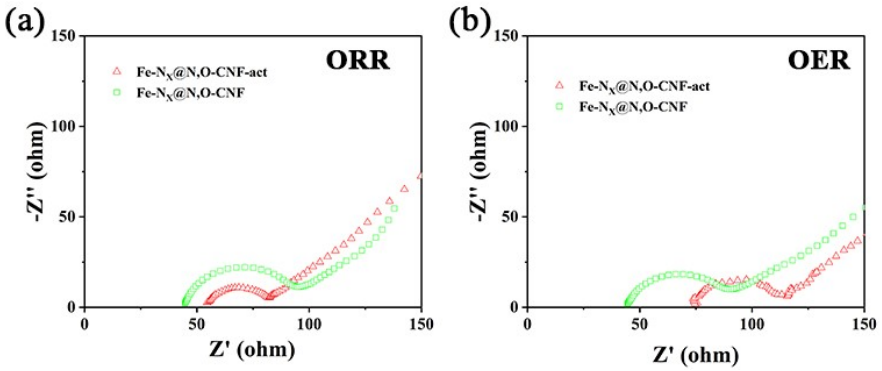

Fig. S8 EIS plots of Fe-N_X@N,O-CNF-act and Fe-N_X@N,O-CNF.

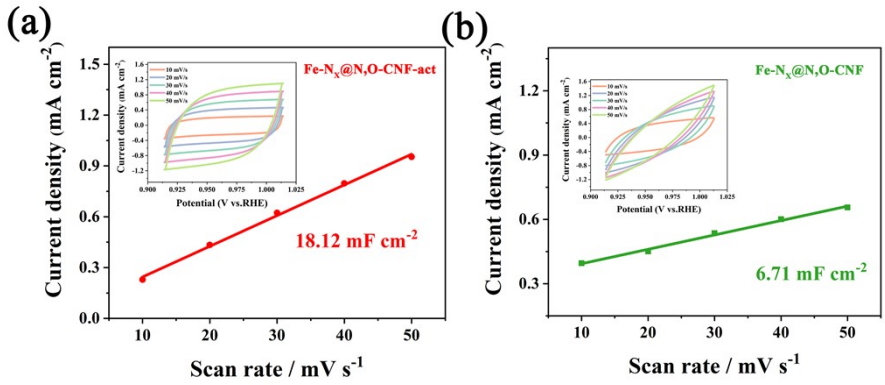

Fig. S9 CV curves at multiple scan rates of (a) Fe-N_X@N,O-CNF-act (b) Fe-N_X@N,O-CNF. Inset: C_{dl} plotted between sweeping speed vs. current density.

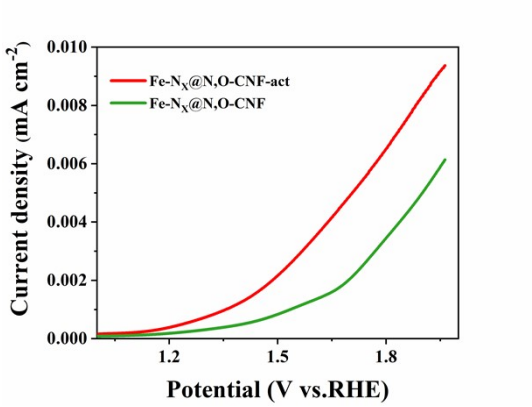

Fig. S10 ECSA corrected OER LSV curves.

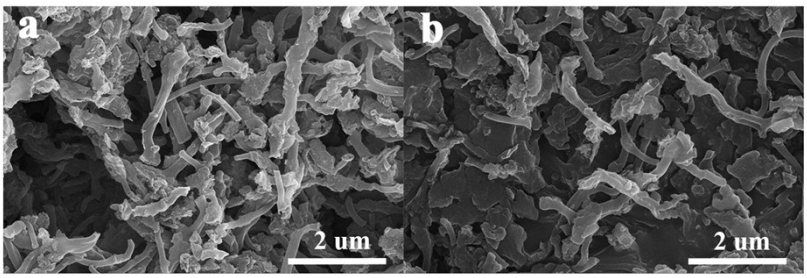

Fig. S11 SEM image of Fe-N$_X$@N,O-CNF-act before (a) and after (b) stability test.

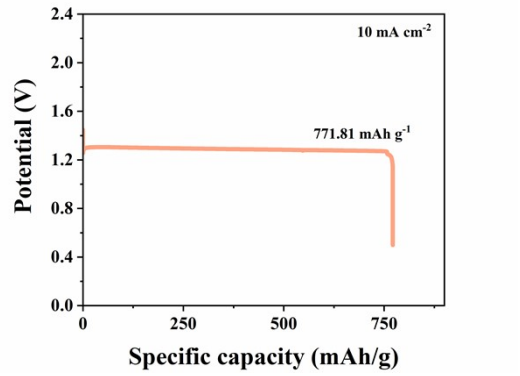

Fig. S12 Specific capacities of Fe-N$_X$@N,O-CNF-act at 10 mA cm^{-2}.

Table S1 The content of N species.

	Pyridine N (%)	Fe-N_X (%)	Pyrrole N (%)	Graphite N (%)	Oxide N (%)
Fe-N_X@N,O-CNF-act	24.17	11.33	23.6	26.66	14.24
Fe-N_X@N,O-CNF	26.63	15.44	34.57	11.78	11.57

Table S2 The content of O species.

	O1 (%)	C=O (%)	O2 (%)	C-O-C (%)
Fe-N_X@N,O-CNF-act	13.98	35.13	36.53	14.38
Fe-N_X@N,O-CNF	24.97	35.78	31.83	7.42

Table S3 ORR and OER performance

	Fe-N_X@N,O-CNF-act	Fe-N_X@N,O-CNF	Pt/C	RuO_2	CNF
E_{oneset} (V)	0.995	0.935	0.967	-	0.913
$E_{1/2}$ (V)	0.872	0.792	0.846	-	0.749
j_l (mA cm^{-2})	5.69	4.01	5.21	-	3.42
Tafel slope (mV dec^{-1})	78.25	79.66	96.67	-	
$E_{j=10}$(V)	1.632	-		1.608	
Tafel slope (mV dec^{-1})	194	507		90.8	

Table S4 The content of element.

	C1s (%)	Fe2p (%)	N1s (%)	O1s (%)
Fe-N_X@N,O-CNF-act	94.73	0.1	2.35	2.82
Fe-N_X@N,O-CNF	96.11	0.06	1.2	2.64

Table S5 ORR and OER performance

	0.25-Fe-N_X@N,O-CNF-act	0.5-Fe-N_X@N,O-CNF-act (This work)	1.0-Fe-N_X@N,O-CNF-act
E_{oneset} (V)	0.999	0.995	0.988
$E_{1/2}$ (V)	0.864	0.872	0.878
j_l (mA cm^{-2})	5.49	5.69	5.9
$E_{overpotential}$	1.628	1.609	1.614